Chapter 6 Wear and Biological Behaviour of Additively Manufactured Ti-6Al-4V Alloy

In this chapter, wear and biological studies are discussed in detail. The width of resulting wear tack was measured and then wear rate is calculated by measuring the mass before and after wear test. This chapter describes the microstructural characterization of wear track and Raman analysis. This chapter also includes the biocompatibility test to evaluate the cell culture behaviour of additively manufactured Ti-6Al-4V samples.

6.1 Results and discussion

6.1.1 Wear track depth and wear rate

Figure 6.1 (a–d) present the variation of wear depth across the wear scar width for the both conventional as well as as-built L-PBF samples, tested at 5 N load with 382 rpm sliding velocity, 5 N with 891 rpm, 25 N with 382 rpm, and 25 N with 891 rpm. The L-PBF AB 90° oriented samples experienced more wear track depth in comparison with 0° and 45° oriented samples.

Figure 6.2 (a–c) present the variation of wear depth across the wear scar width for heat-treated L-PBF samples tested at 5 N load with 382 rpm sliding velocity, 5 N with 891 rpm, 25 N with 382 rpm, and 25 N with 891 rpm. Furthermore, Figure 6.2 (d) presents the overall trend of the maximum wear depth observed in all the samples. Volumetric wear depends upon both the wear scar width and wear track depth. With an increase in the applied load, there is an increase in the wear depth, consequently increasing the volumetric wear.

Across all the samples, except for the as-built L-PBF 0° sample, wear depth reaches its peak at 25 N and 382 rpm. However, the aforementioned L-PBF 0° sample exhibits its maximum wear depth under conditions of 25 N and 891 rpm, as shown in Figure 6.2 (d). The wear tracks of conventional and L-PBF AB samples (Figure 6.1) reveal a rougher appearance than that of L-PBF HT samples (Figure 6.2).

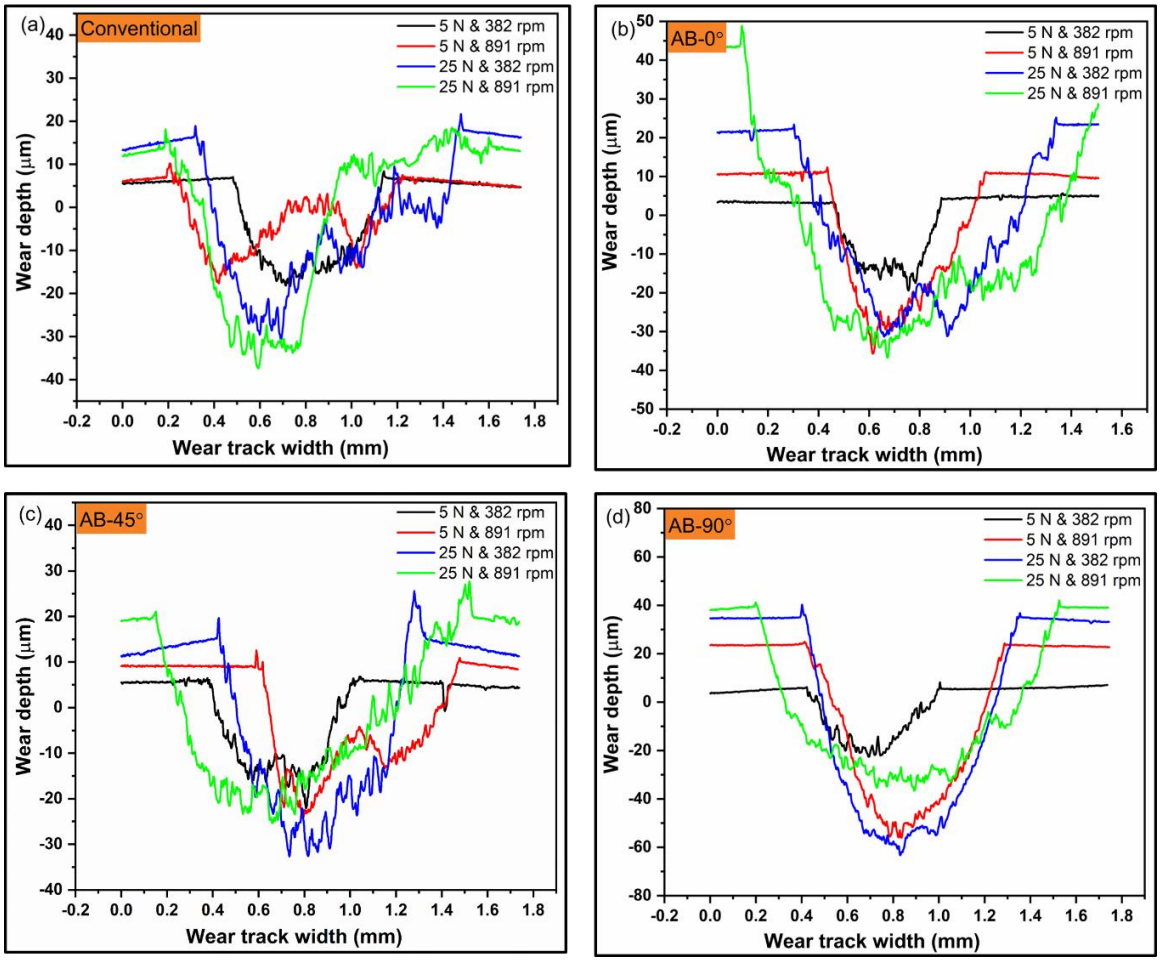

Figure 6.1 Variation of wear track depth across wear scar width for: (a) Conventional, (b) L-PBF AB-0°, (c) L-PBF AB-45°, (d) L-PBF AB-90° samples

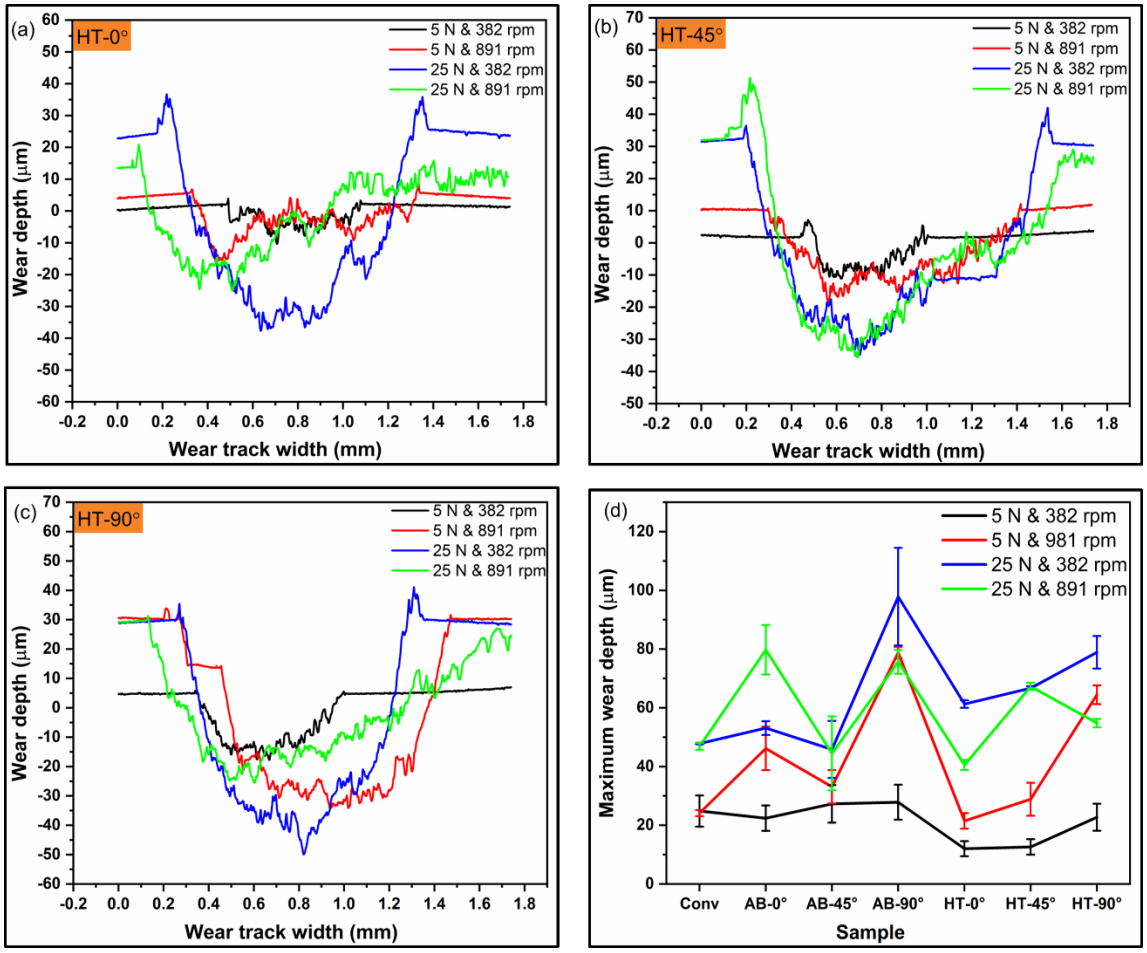

Figure 6.2 Variation of wear track depth across wear scar width for L-PBF samples: (a) HT-0°, (b) HT-45°, (c) HT-90°, and (d) trend of maximum wear depth of all wear samples

Figure 6.3 shows the wear rates observed in the both conventional as well as L-PBF samples across different orientations, loads, and sliding velocities. For same load, if sliding velocity increases wear rate decreases for the AB and HT conventional and L-PBF samples in all orientations. Similarly, an increase in load, while maintaining a constant velocity, amplifies wear rates uniformly in AB and HT conventional as well as L-PBF samples across various orientations.

A nuanced pattern emerges concerning the effect of build orientation on wear rates. Initially, for AB samples at low loads and sliding velocities, wear rates exhibit a

decreasing trend as build orientation progresses from 0° to 90°, followed by an eventual rise. Notably, the wear rate of the AB L-PBF samples surpasses that of conventional samples. However, after the heat treatment, the wear rates of L-PBF samples align comparably with those of the conventional samples.

At low loads and sliding velocities, the maximum wear rate is in the 90° orientation, followed by the 0° orientation, while the 45° orientated sample demonstrates the minimum wear rate. This trend alters at higher loads and sliding velocities, displaying a change in the wear rate sequence across orientations. Specifically, at 5 N load and 382 rpm, the wear rate sequence from highest to lowest is: AB-90° (2.876×10^{-6} mm^3/mm) > AB-0° (2.551×10^{-6} mm^3/mm) > Conv (2.369×10^{-6} mm^3/mm) > AB-45° (1.879×10^{-6} mm^3/mm). This pattern shifts at 25 N and 891 rpm, with the sequence being: AB-90° (7.482×10^{-6} mm^3/mm) > AB-0° (6.647×10^{-6} mm^3/mm) > AB-45° (5.568×10^{-6} mm^3/mm) > Conv (3.465×10^{-6} mm^3/mm) (Table 6.1).

Notably, across all the samples, the maximum wear rate occurs consistently at 25 N and 382 rpm. The order of wear rate under these conditions is: AB-90° (10.933×10^{-6} mm^3/mm) > AB-45° (9.874×10^{-6} mm^3/mm) > AB-0° (9.645×10^{-6} mm^3/mm) > Conv (7.858×10^{-6} mm^3/mm). This observed wear rate behaviour can be attributed to complex relation between the build orientation, load, and sliding velocity, influencing the surface characteristics and frictional interactions between the samples during wear testing process.

Following the heat treatment, as the build orientation increases from 0° to 90°, initially wear rate of the L-PBF samples increases then decreases across load and sliding velocity conditions. Specifically, at 5 N load and 382 rpm, the descending order of wear rates is: Conv (2.369×10^{-6} mm^3/mm) > HT-45° (2.104×10^{-6} mm^3/mm) > HT-0° (1.794×10^{-6}

mm^3/mm) > HT-90° (1.765 x 10^{-6} mm^3/mm). At a higher load of 25 N and 891 rpm, the wear rates are in following order: HT-45° (4.762 x 10^{-6} mm^3/mm) > Conv (3.465 x 10^{-6} mm^3/mm) > HT-90° (3.100 x 10^{-6} mm^3/mm) > HT-0° (2.548 x 10^{-6} mm^3/mm).

Notably, across all the conditions, the highest wear rates observed at 25 N load and 382 rpm, with the sequence: HT-90° (9.338 x 10^{-6} mm^3/mm) > HT-0° (8.635 x 10^{-6} mm^3/mm) > HT-45° (8.471 x 10^{-6} mm^3/mm) > Conv (7.858 x 10^{-6} mm^3/mm). The wear rates exhibited by the heat-treated samples were comparatively lower than those of their as-built counterparts. These results suggest a complex interplay between build orientation, applied load, and sliding velocity, significantly impacting wear characteristics in L-PBF components following heat treatment.

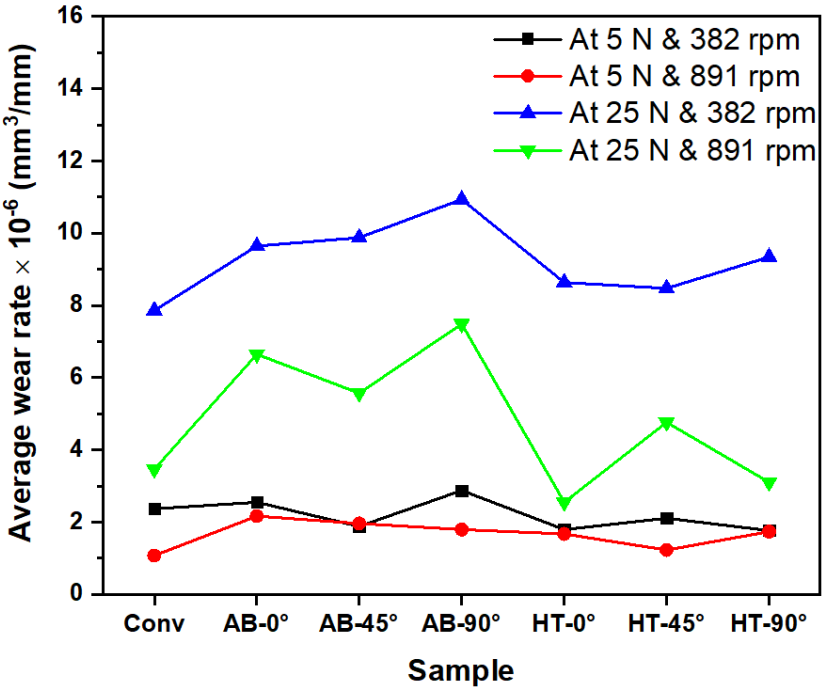

Figure 6.3 Average wear rate of conventional and L-PBF Ti-6Al-4V samples in each condition after 45 minutes at 5 N with 382 rpm, 5 N with 891 rpm, 25 N with 382 rpm, and 25 N with 891 rpm, respectively

Table 6.1 Average wear rate of the conventional and L-PBF Ti-6Al-4V samples at different combinations of applied load and sliding velocity

Sample	Average wear rate x 10^{-6} (mm^3/mm)			
	At 5 N and 382 rpm	At 5 N and 891 rpm	At 25 N and 382 rpm	At 25 N and 891 rpm
Conv.	2.369	1.075	7.858	3.465
AB-0°	2.551	2.164	9.645	6.647
AB-45°	1.879	1.960	9.874	5.568
AB-90°	2.876	1.794	10.933	7.482
HT-0°	1.794	1.670	8.635	2.548
HT-45°	2.104	1.227	8.471	4.762
HT-90°	1.765	1.733	9.338	3.100

6.1.2 Coefficient of friction (COF)

Figure 6.4 (a-d) shows the coefficient of friction (COF) profiles over time for conventionally and additively manufactured samples, built in different conditions, at different sliding velocities and loads. The coefficient of friction of all the samples stabilizes after 1500 s and maintains a constant value throughout the remaining test duration with minimal fluctuations in the amplitude. The trend of average coefficient of friction for the different samples is shown in Figure 6.5 and presented in Table 6.2.

From Figure 6.4, it is evident that the as build orientation increases from 0° to 90°, COF of the L-PBF as-built samples increases at each load and sliding velocity, except at 5 N and 891 rpm, where the COF initially increases and then decreases. Notably, across all the conditions, the highest COF was observed at 5 N load and 382 rpm in the as-built L-PBF samples, with the sequence being: AB-90° (0.439) > AB-45° (0.435) > AB-0° (0.287). At a higher load of 25 N and increased sliding velocity of 891 rpm, the COF shows the following order: AB-90° (0.362) > AB-45° (0.346) > AB-0° (0.253). The COF of conventional samples lies between the COF of AB-0° and AB-45°.

Following heat treatment, as build orientation increases from 0° to 90°, the COF of the L-PBF samples increases at each load and sliding velocity except at 5 N load and 382 rpm where the COF decreases as build orientation increases from 0° to 90°. At 5 N load and

382 rpm, the descending order of COF is: HT-0° (0.596) > HT-45° (0.565) > HT-90° (0.460). At a higher load of 25 N and 891 rpm, the COF presents following order: HT-90° (0.445) > HT-45° (0.410) > HT-0° (0.374).

In addition, across all the conditions, the highest COF observed at 5 N load and 382 rpm sliding velocity in the heat-treated L-PBF samples. After heat treatment, the COF of 0° and 45° oriented L-PBF samples significantly increased by 107.66 % and 29.88 % respectively at 5 N load and 382 rpm sliding velocity and 47.83 % and 18.49 % respectively at 25 N load and 891 rpm sliding velocity. The COF of 90° oriented L-PBF samples increased by 4.78 % only at 5 N load and 382 rpm sliding velocity and significantly increased by 22.83 % at 25 N load and 891 rpm sliding velocity.

The COF exhibited by heat-treated samples were comparatively higher than those of their as-built counterparts, attributing this increment to the improved wear resistance and more adhesion evident in the heat-treated specimens.

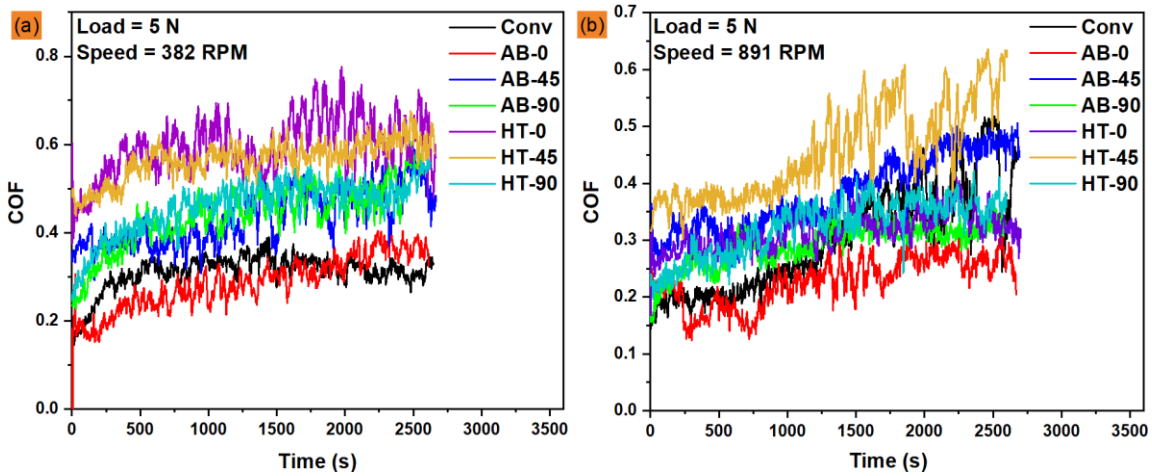

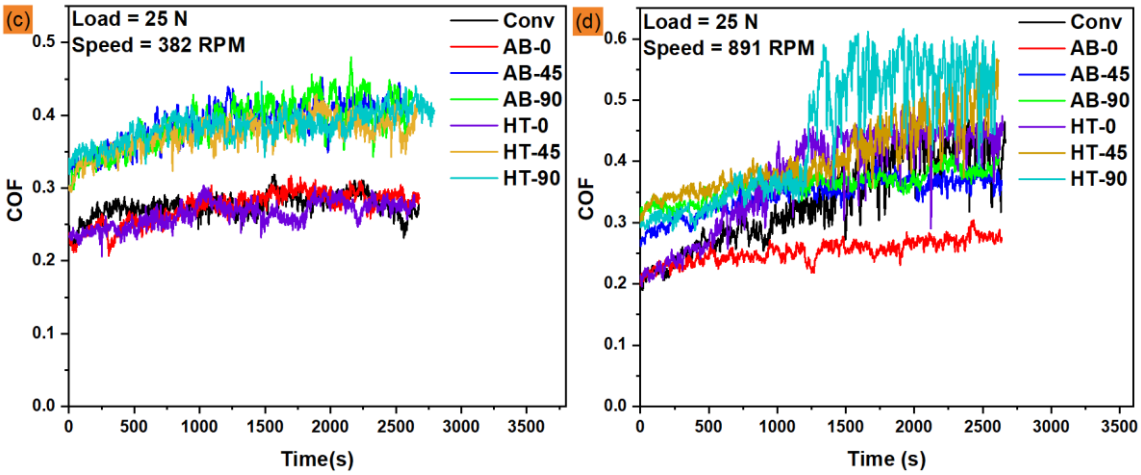

Figure 6.4 Evolution of COF with time for conventional and L-PBF processed Ti-6l-4V samples: (a) at 5 N and 382 RPM, (b) at 5 N and 891 RPM, (c) at 25 N and 382 RPM, and (d) at 25 N and 891 RPM

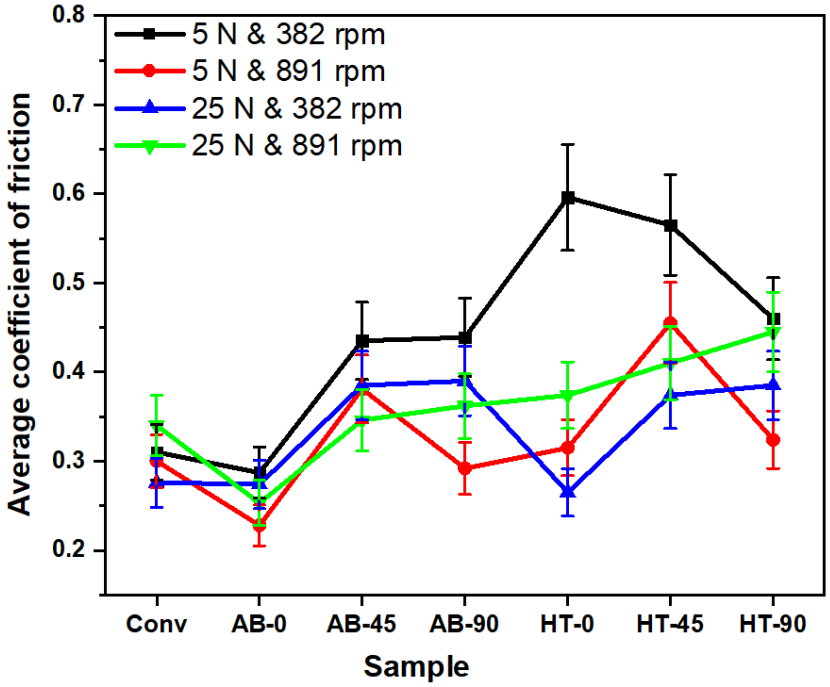

Figure 6.5 Average coefficient of friction of conventional and L-PBF AB and HT samples after 45 minutes at 5 N with 382 rpm, 5 N with 891 rpm, 25 N with 382 rpm, and 25 N with 891 rpm

Table 6.2 Average coefficient of friction of the conventional and L-PBF samples at different loads and sliding velocities

Sample	Average coefficient of friction			
	At 5 N and 382 rpm	At 5 N and 891 rpm	At 25 N and 382 rpm	At 25 N and 891 rpm
Conv.	0.310	0.300	0.276	0.340
AB-0°	0.287	0.228	0.274	0.253
AB-45°	0.435	0.381	0.385	0.346
AB-90°	0.439	0.292	0.390	0.362
HT-0°	0.596	0.315	0.265	0.374
HT-45°	0.565	0.455	0.374	0.410
HT-90°	0.460	0.324	0.385	0.445

6.1.3 Microstructural characterization of the wear track surfaces of the conventional and AM samples

Figure 6.6 (a-h) presents wear track micrographs resulting from conventional samples after the wear test against zirconia ball at different loads and sliding velocities. Figure 6.6 (a, c, e, and g) show the wear track width formed on the surfaces at 5 N with 382 rpm, 5 N with 891 rpm, 25 N with 382 rpm, and 25 N with 891 rpm respectively.

It can be noted that the largest wear track width was found on conventional samples tested at 25 N load and 891 rpm sliding velocity. Figure 6.6 shows that grooves are present on all the conventional samples, due to formation of abrasive wear. Figure 6.6 (b, d, f, and h) shows the enlarge view of different worn surfaces shown in Figure 6.6 (a, c, e, and g) respectively. Figure 6.6 also presents EDS spectrum and weight % of different elements observed on worn surfaces of the conventional samples. The conventional worn samples exhibit grooves along sliding direction, oxidized particles, and delamination at each load and sliding velocity. The formation of oxides on the worn surfaces has been confirmed by the elemental maps shown in Figure 6.6.

At high load and sliding velocity, it exhibits adhesive wear also (Figure 6.6 (h)) and it has been confirmed by significant presence of zirconia weight % in elemental map. The

presence of higher content of oxygen in each condition (elemental distribution shown in Figure 6.6) results in formation of more protective layers and may have contributed in lowering the wear rate (Table 6.1) compared to the L-PBF samples at each load and sliding velocity condition.

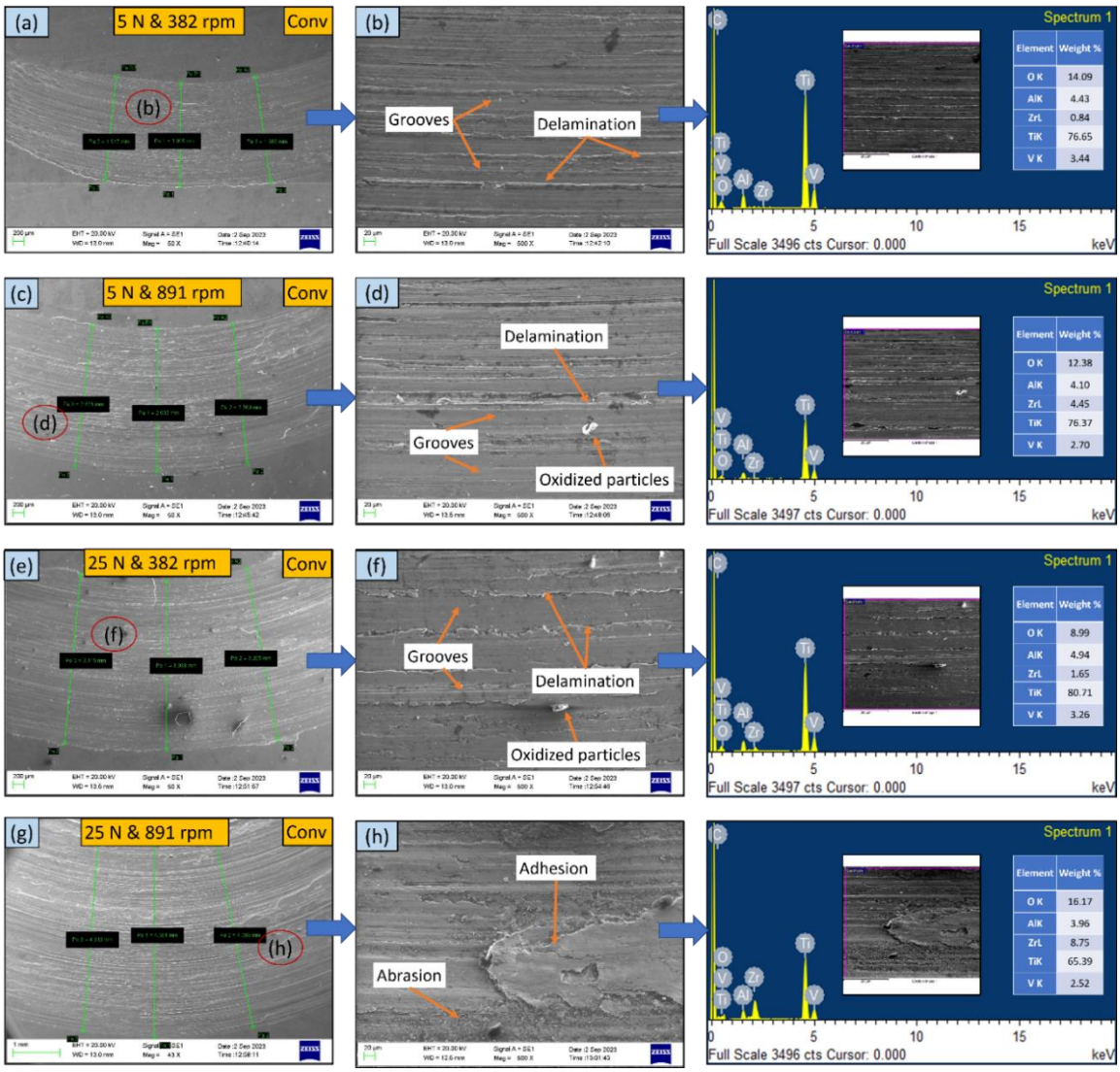

Figure 6.6 SEM micrographs with EDS spectrum of worn surfaces of Ti-6Al-4V conventional samples tested at: (a, b) 5 N with 382 rpm, (c, d) 5 N with 891 rpm, (e, f) 25 N with 382 rpm, and (g, h) 25 N with 891 rpm

Figure 6.7 - Figure 6.9 (a-h) present worn surface micrographs of the L-PBF AB-0°, 45°, and 90° oriented samples respectively at different loads and sliding velocities. Figure 6.7

- Figure 6.9 (a, c, e, and g) show the wear track width formed on the surfaces at 5 N with 382 rpm, 5 N with 891 rpm, 25 N with 382 rpm, and 25 N with 891 rpm respectively. Figure 6.7 - Figure 6.9 (b, d, f, and h) show the enlarge view of different worn surfaces shown in Figure 6.7 - Figure 6.9 (a, c, e, and g) respectively.

Figure 6.7 - Figure 6.9 also present the EDS spectrum and weight % of different elements observed on worn surfaces of L-PBF AB-0°, 45°, and 90° oriented samples respectively at different loads and sliding velocities. It is observed that the largest wear track width was found on all the L-PBF AB samples tested at 25 N load and 891 rpm sliding velocity. The AB 0° worn samples exhibit evidence of delamination, grooves, transfer layer, oxidized particles at each load and sliding velocity (Figure 6.7 (b, d, f, and h)).

The AB 45° worn samples also exhibit evidence of deep grooves, abrasive wear, oxidized particles at each load and sliding velocity (Figure 6.8 (b, d, f, and h)). At high load and sliding velocity, the AB 45° sample exhibit significant transfer of zirconia on the Ti-6Al-4V samples and it has been confirmed by the presence of zirconia weight % in elemental distribution map.

The AB 90° worn samples show the presence of delamination, grooves, and oxidized particles at each load and sliding velocity (Figure 6.9 (b, d, f, and h)). In AB 90° worn samples, significant transfer of material is not observed which is confirmed by the minor presence of zirconia weight % in elemental distribution map. This may have contributed to the smooth surface but high wear rate compared to AB 45° samples (Table 6.1).

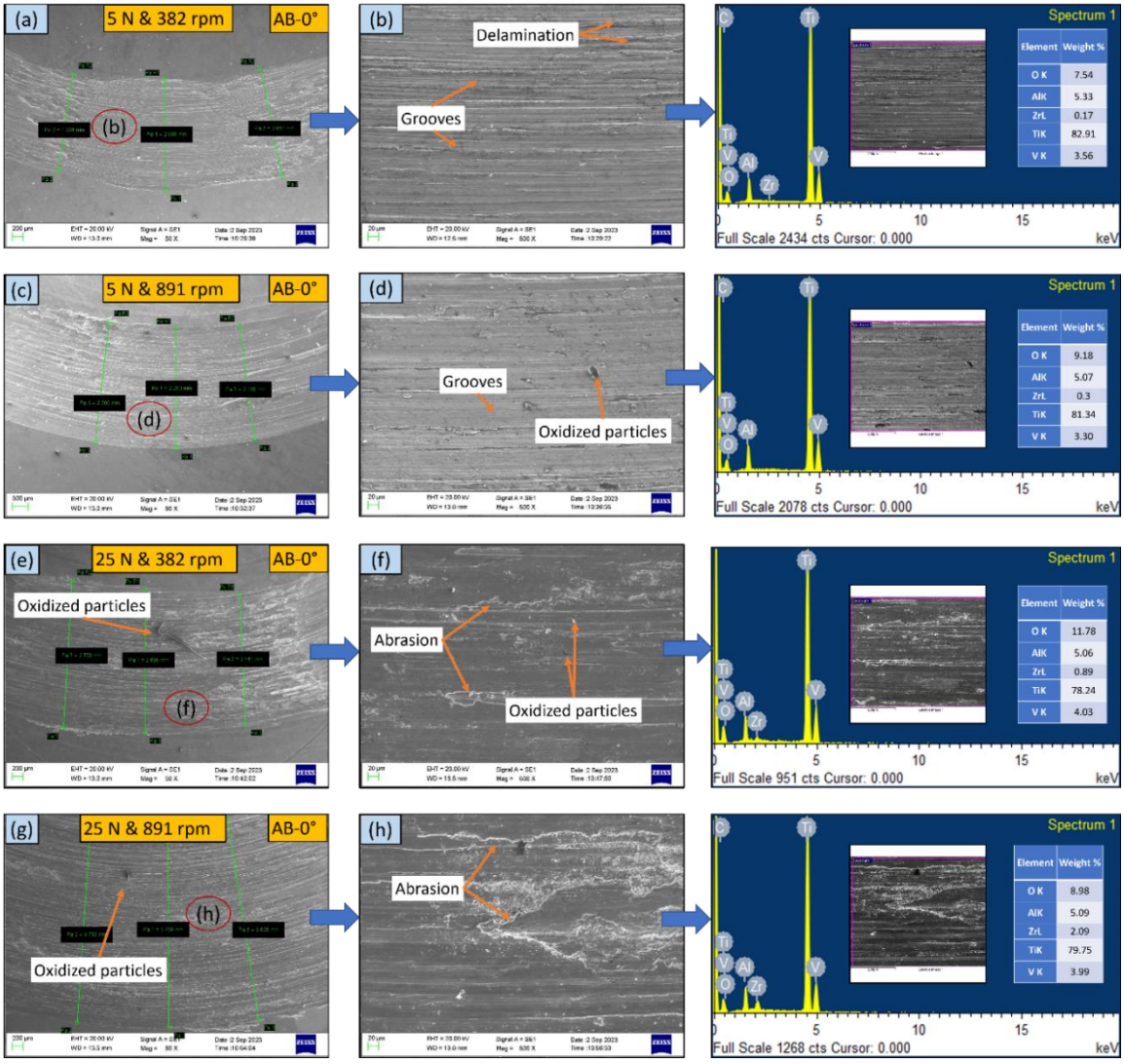

Figure 6.7 SEM micrographs with EDS spectrum of worn surfaces of Ti-6Al-4V AM as-built 0° orientated specimens tested at: (a, b) 5 N with 382 rpm, (c, d) 5 N with 891 rpm, (e, f) 25 N with 382 rpm, and (g, h) 25 N with 891 rpm

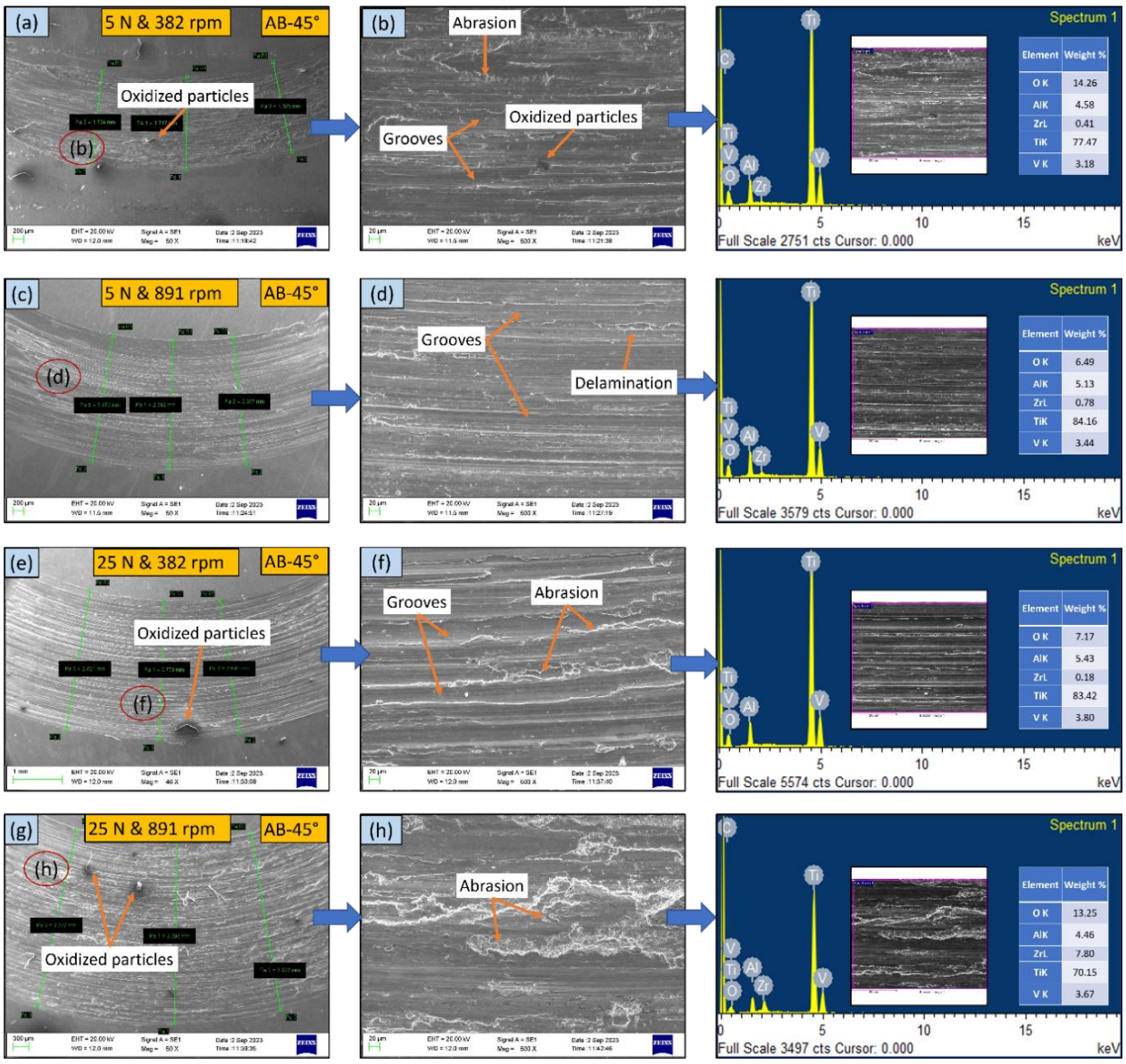

Figure 6.8 SEM micrographs with EDS spectrum of worn surfaces of Ti-6Al-4V AM as-built 45° orientated specimens tested at: (a, b) 5 N with 382 rpm, (c, d) 5 N with 891 rpm, (e, f) 25 N with 382 rpm, and (g, h) 25 N with 891 rpm

Figure 6.10 - Figure 6.12 (a-h) present worn surface micrographs of the L-PBF HT-0°, 45°, and 90° oriented samples respectively, at different loads and sliding velocities. Figure 6.10 - Figure 6.12 (a, c, e, and g) show the wear track width formed on the surfaces at 5 N with 382 rpm, 5 N with 891 rpm, 25 N with 382 rpm, and 25 N with 891

rpm respectively. Figure 6.10 - Figure 6.12 (b, d, f, and h) show the enlarge view of different worn surfaces shown in Figure 6.10 - Figure 6.12 (a, c, e, and g) respectively.

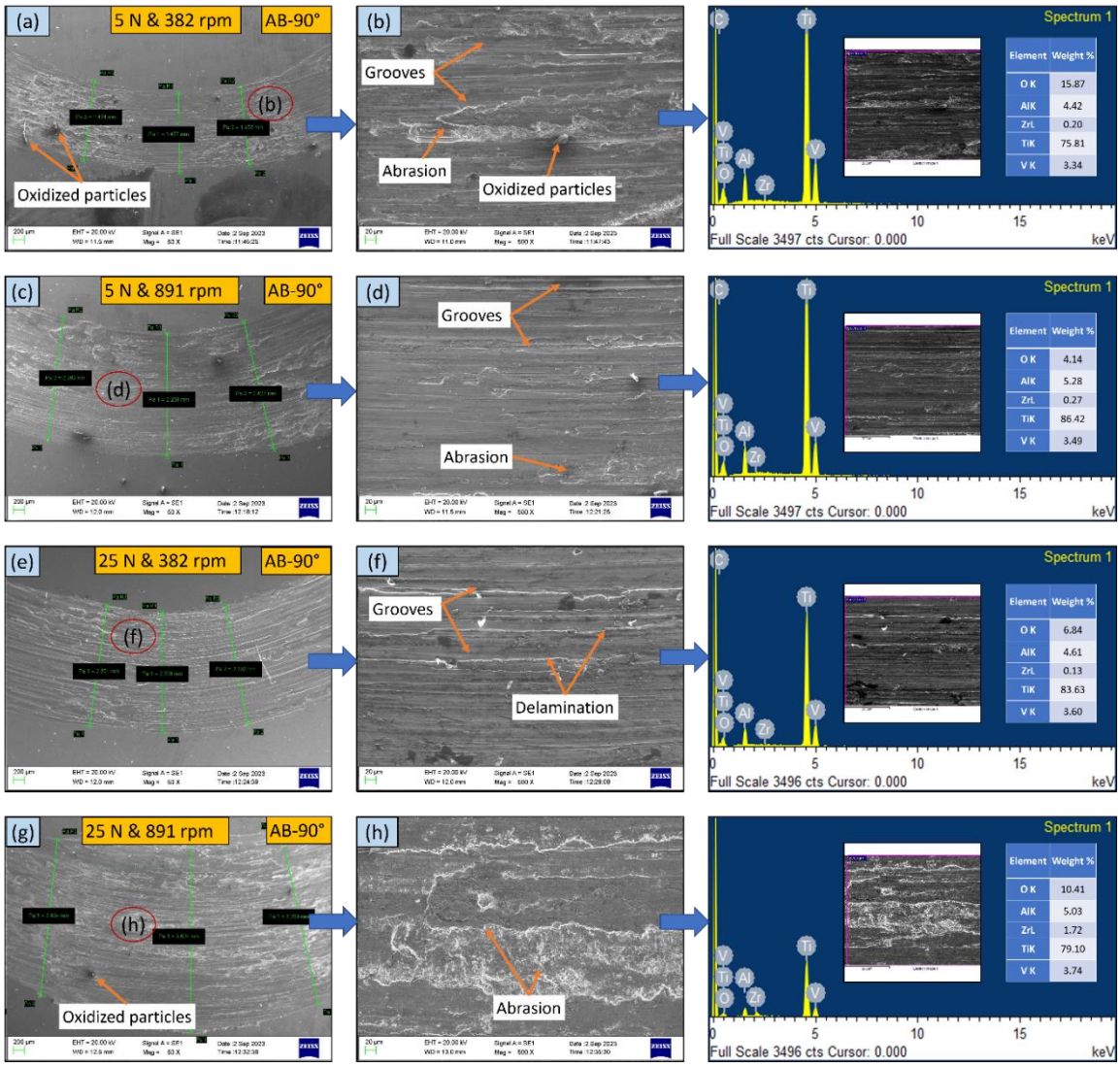

Figure 6.9 SEM micrographs with EDS spectrum of worn surfaces of Ti-6Al-4V AM as-built 90° orientated specimens tested at: (a, b) 5 N with 382 rpm, (c, d) 5 N with 891 rpm, (e, f) 25 N with 382 rpm, and (g, h) 25 N with 891 rpm

Figure 6.10 - Figure 6.12 also present the EDS spectrum and weight % of different elements observed in worn surfaces of the L-PBF HT-0°, 45°, and 90° oriented samples respectively, at different loads and sliding velocities. After heat treatment, largest wear track width was observed at 25 N load and 891 rpm sliding velocity in all the L-PBF HT

samples. The build orientation has no effect on worn surfaces but the effect of heat treatment is observed. Some adhesive wear was observed in the heat-treated samples.

The HT 0° worn samples exhibited more oxidized particles than HT 45° and 90° worn samples. The HT 90° worn samples revealed abrasion, delamination, and grooves at each load and sliding velocity (Figure 6.12 (b, d, f, and h)). At high load and sliding velocity, the HT 45° sample exhibited significant transfer of zirconia on the Ti-6Al-4V samples and that was confirmed by the presence of zirconia weight % in elemental distribution map (Figure 6.11 (g)). The HT 0° worn samples exhibited more weight % of oxygen which formed protective layers of titanium oxide on surface of the Ti-6Al-4V samples, hence the wear rate was lower in comparison with those of HT 45° and HT 90° samples (Table 6.1).

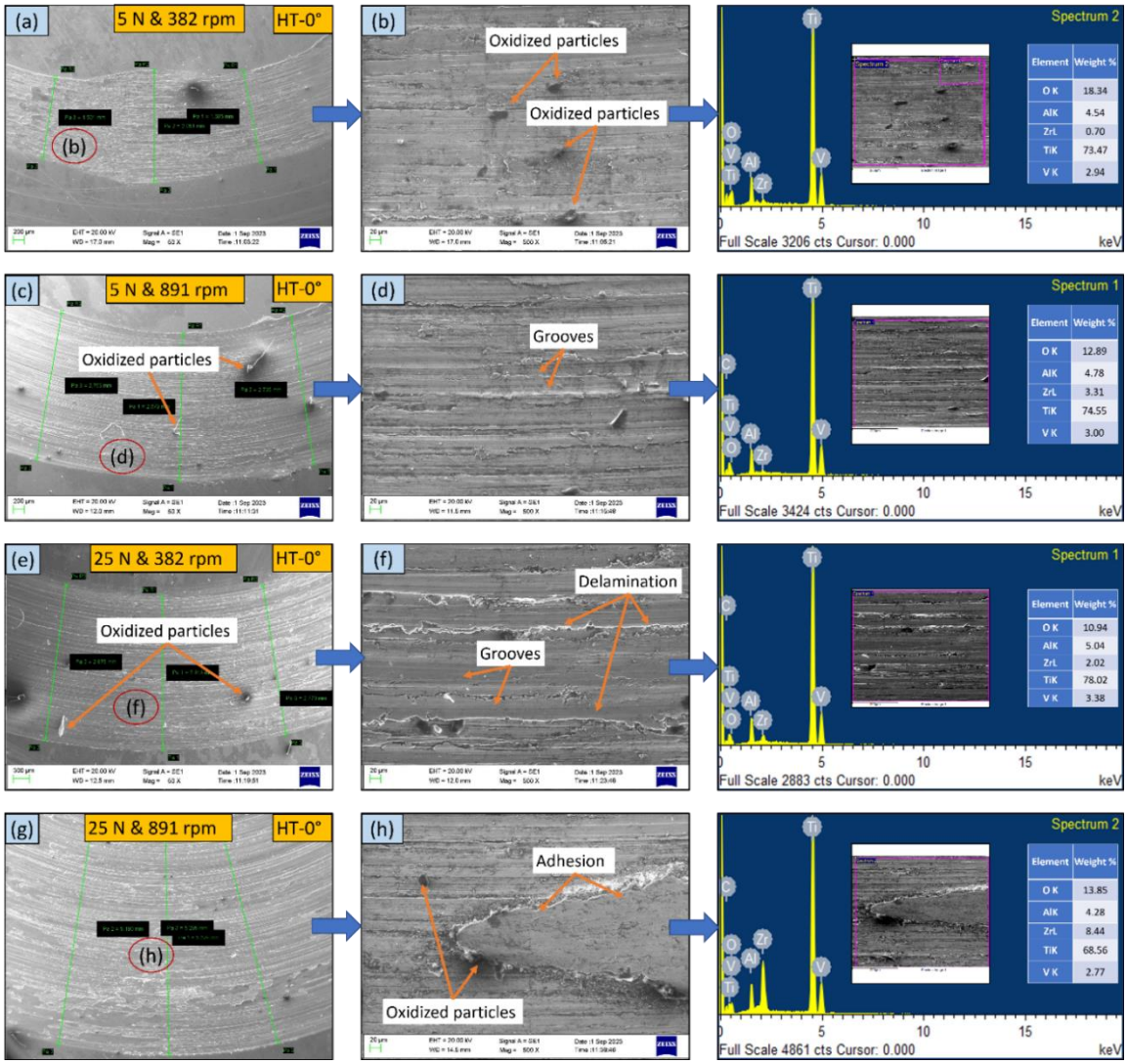

Figure 6.10 SEM micrographs with EDS spectrum of worn surfaces of Ti-6Al-4V AM heat-treated 0° orientated specimens tested at: (a, b) 5 N with 382 rpm, (c, d) 5 N with 891 rpm, (e, f) 25 N with 382 rpm, and (g, h) 25 N with 891 rpm

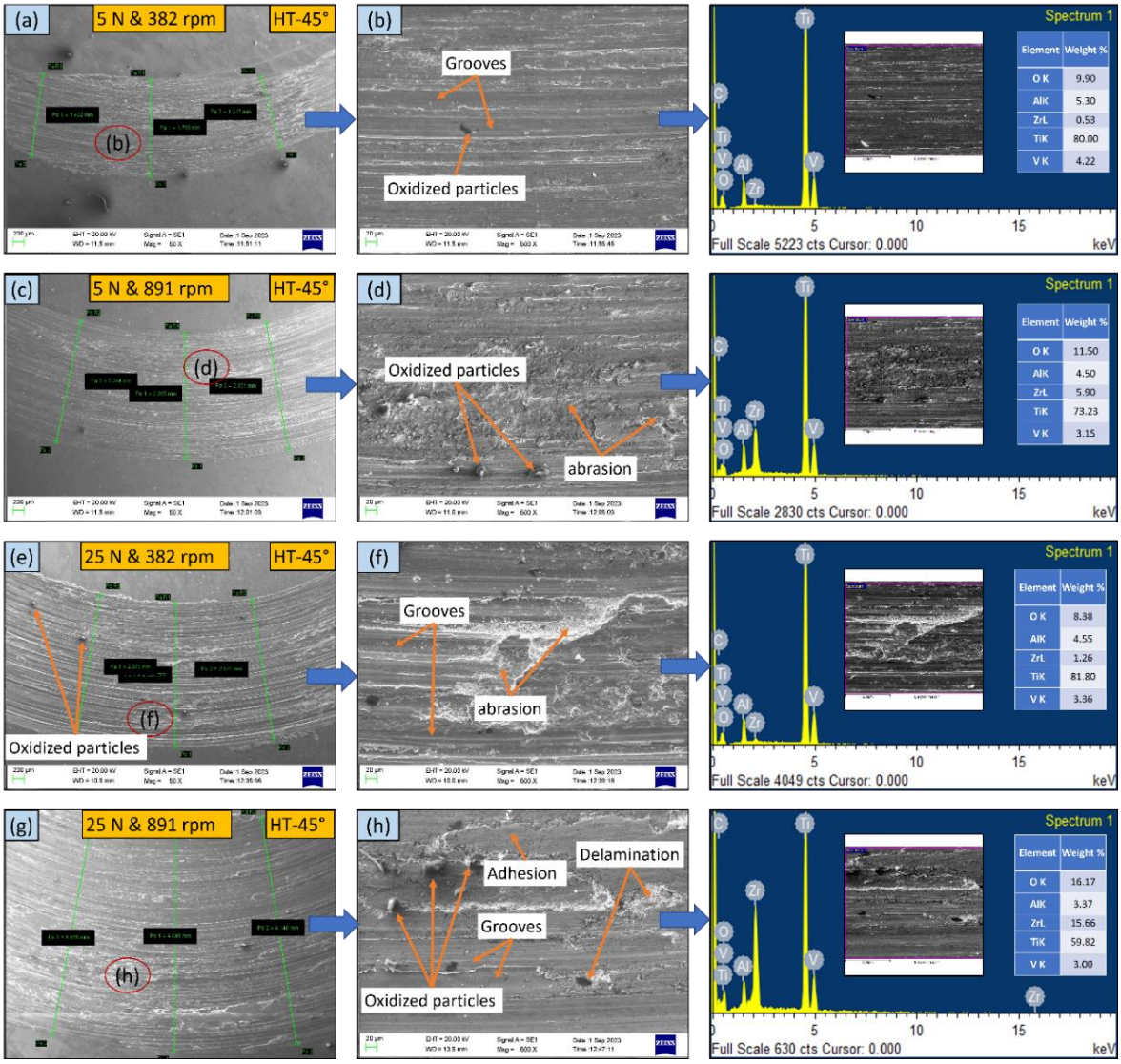

Figure 6.11 SEM micrographs with EDS spectrum of worn surfaces of Ti-6Al-4V AM heat-treated 45° orientated specimens tested at: (a, b) 5 N with 382 rpm, (c, d) 5 N with 891 rpm, (e, f) 25 N with 382 rpm, and (g, h) 25 N with 891 rpm

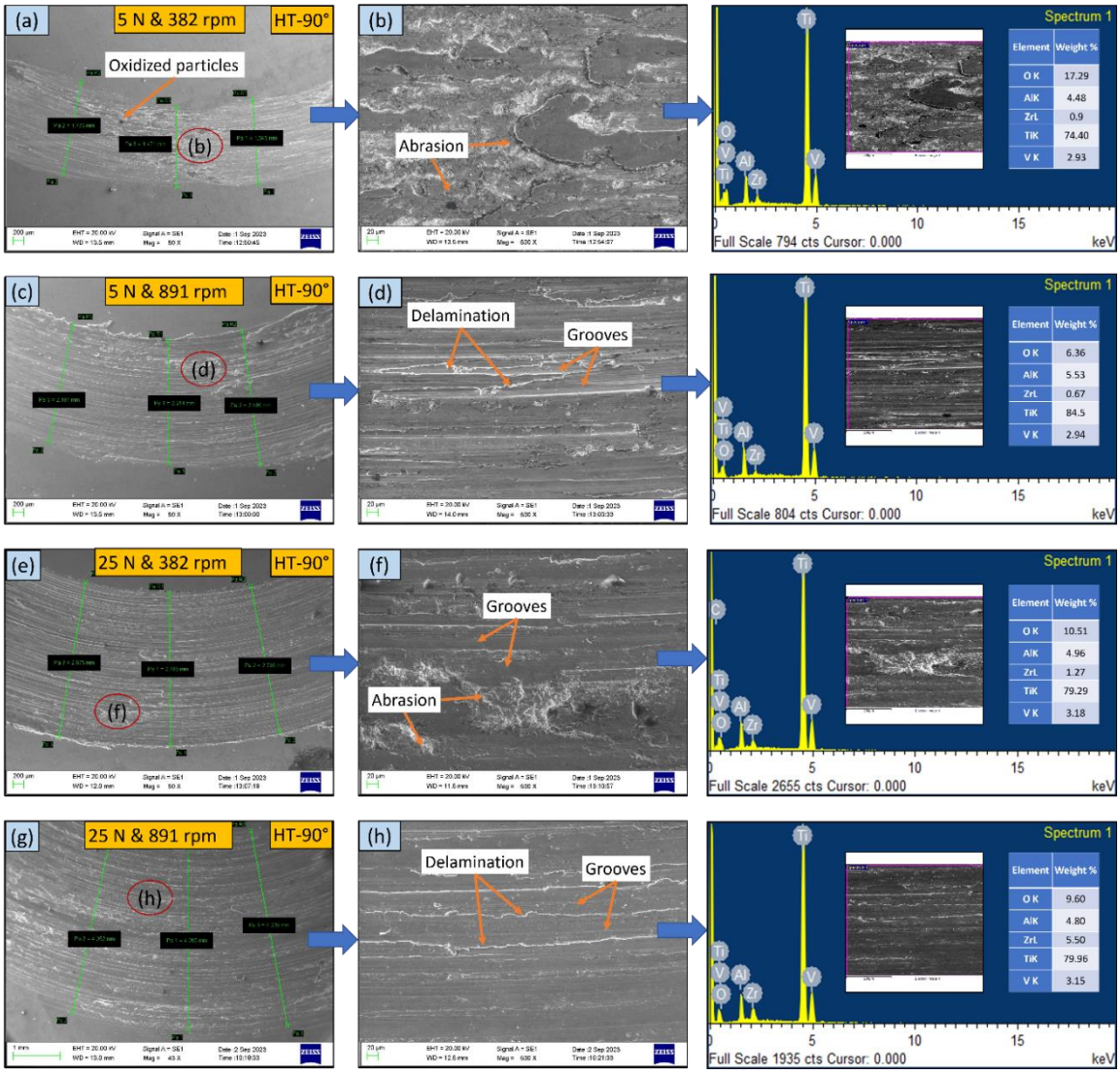

Figure 6.12 SEM micrographs with EDS spectrum of worn surfaces of Ti-6Al-4V AM heat-treated 90° orientated specimens tested at: (a, b) 5 N with 382 rpm, (c, d) 5 N with 891 rpm, (e, f) 25 N with 382 rpm, and (g, h) 25 N with 891 rpm

Figure 6.13 and Figure 6.14 (a-d) show the area maps of worn surfaces of Ti-6Al-4V conventional, AB-0°, AB-45°, and AB-90° samples tested at 5 N load and 382 rpm sliding velocity, at 25 N load and 891 rpm sliding velocity respectively. At low load and low sliding velocity, abrasive wear is observed because transfer of zirconia on Ti-6Al-4V samples was not experienced, it was also confirmed by area map shown in Figure 6.13.

The AB-45° worn samples exhibited small quantity of zirconia, tested at 25 N load and 891 rpm sliding velocity, as shown in Figure 6.14 (c). Figure 6.15 and Figure 6.16 (a-c) show the area maps of worn surfaces of Ti-6Al-4V HT-0°, HT-45°, and HT-90° samples tested at 5 N load and 382 rpm sliding velocity, at 25 N load and 891 rpm sliding velocity respectively. The HT-45° worn samples exhibited larger presence of zirconia on the Ti-6Al-4V samples, which confirmed the adhesive wear.

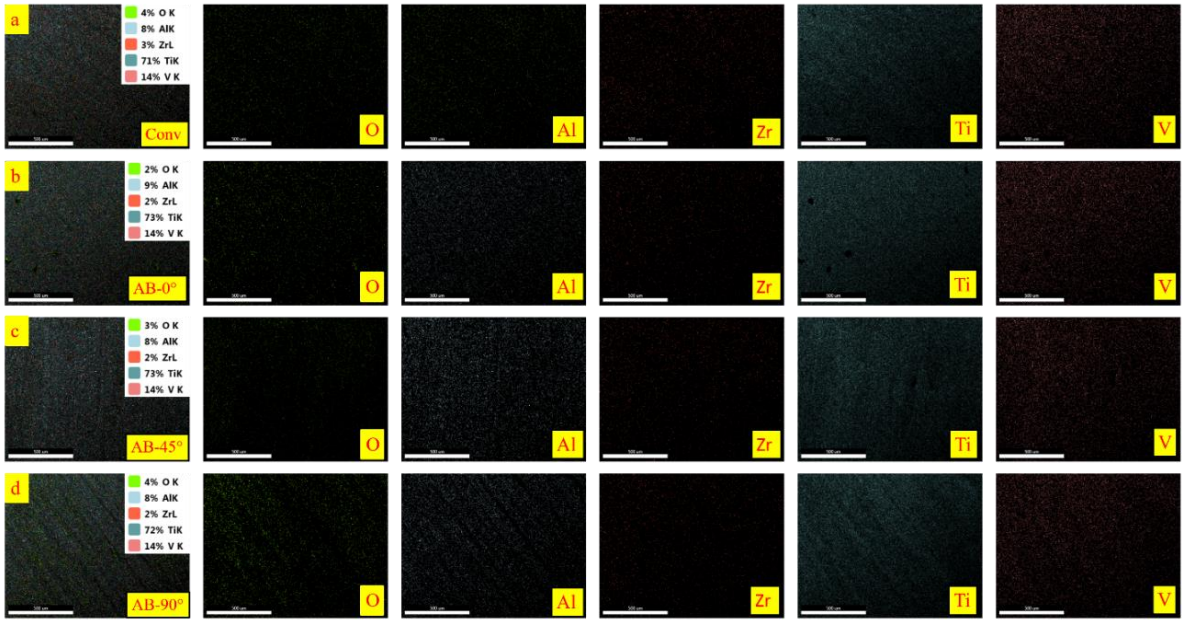

Figure 6.13 Area maps of worn surfaces of Ti-6Al-4V samples tested at 5 N and 382 rpm: (a) conventional, (b) AB-0°, (c) AB-45°, and (d) AB-90°

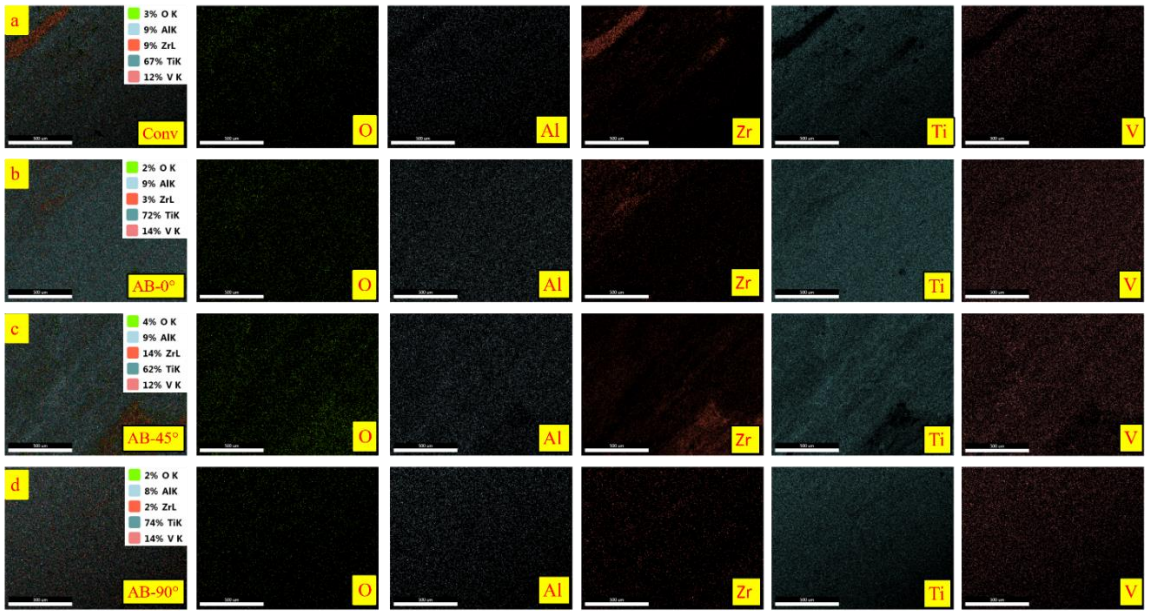

Figure 6.14 Area maps of worn surfaces of Ti-6Al-4V samples tested at 25 N and 891 rpm: (a) conventional, (b) AB-0°, (c) AB-45°, and (d) AB-90°

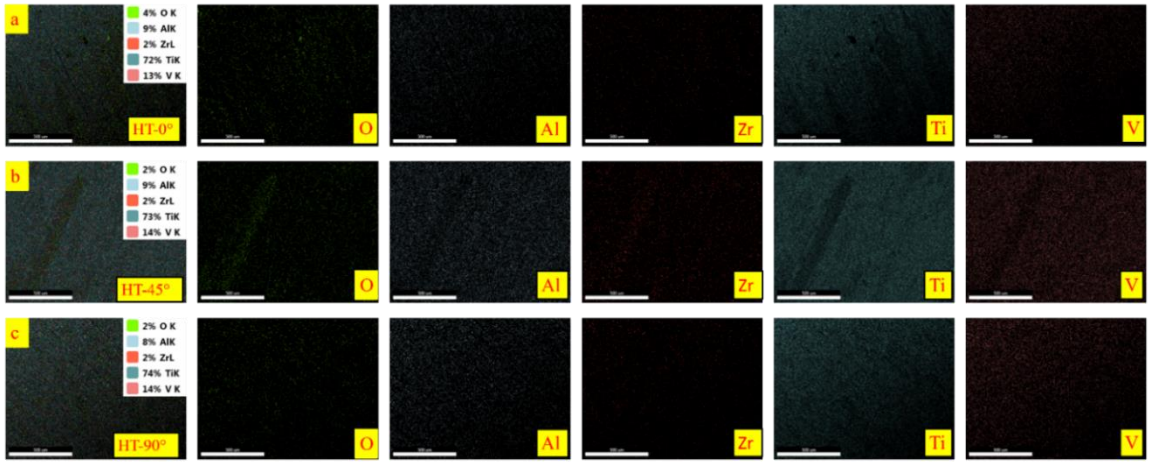

Figure 6.15 Area maps of worn surfaces of Ti-6Al-4V samples tested at 5 N and 382 rpm: (a) HT-0°, (b) HT-45°, and (c) HT-90°

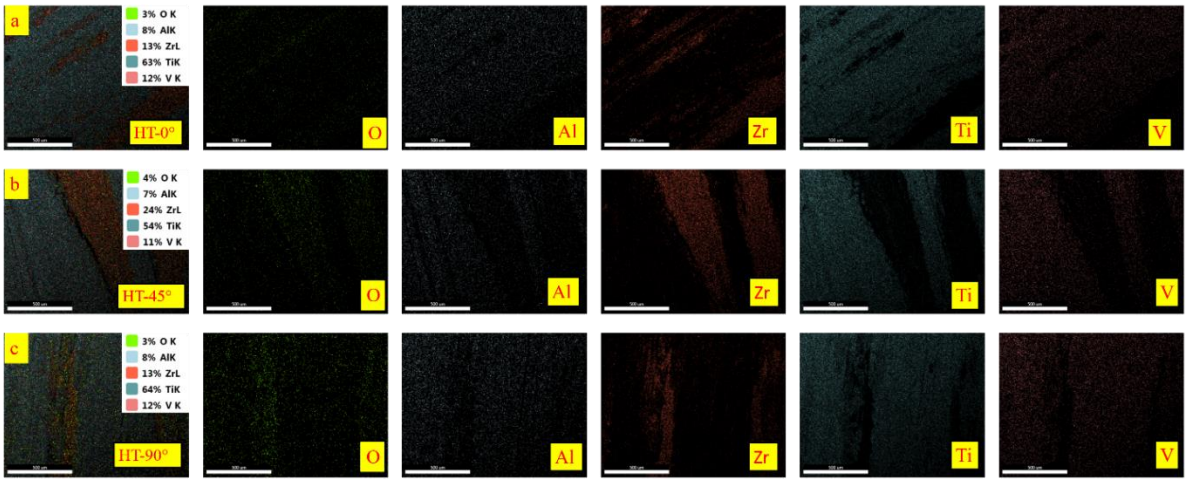

Figure 6.16 Area maps of worn surfaces of Ti-6Al-4V samples tested at 25 N and 891 rpm: (a) HT-0°, (b) HT-45°, and (c) HT-90°

6.1.4 Microstructural characterization of worn surfaces of counter zirconia ball

SEM micrographs and EDS spectra of the zirconia ball's surfaces, following sliding against Ti-6Al-4V samples under various loads and sliding velocities, are depicted in Figure 6.17. Figure 6.18 (a-c) shows the area map of worn surfaces of counter zirconia ball at 5 N and 382 rpm, at 25 N and 382 rpm, at 25 N and 891 rpm, respectively. EDS analysis indicated material transfer from the Ti-6Al-4V plates to zirconia ball, which was evident across all analysed sliding pairs.

The analysis revealed presence of Zr and O from the zirconia ball, alongside Ti, V, and Al originating from the Ti-6Al-4V plates. Additionally, elemental mapping of worn surfaces on the zirconia ball, at different conditions (5 N and 382 rpm, 25 N and 382 rpm, and 25 N and 891 rpm) is presented in Figure 6.18. These maps further illustrate the transfer of material from the Ti-6Al-4V plate to the zirconia ball. Specifically, at 5 N and 382 rpm, a higher weight percentage of Ti is observed in the zirconia ball (Figure 6.18

(a)), while the least weight percentage of Ti is detected at 25 N and 382 rpm (Figure 6.18 (c)).

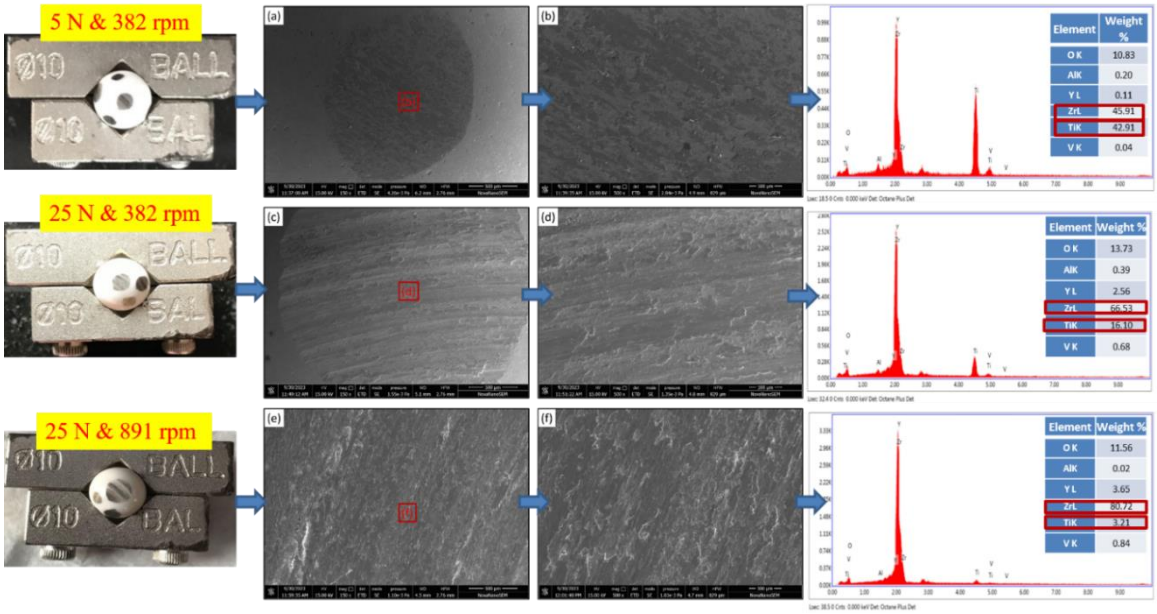

Figure 6.17 SEM micrographs with corresponding EDS spectrum of worn surfaces of counter zirconia ball at: (a) 5 N and 382 rpm, (b) 25 N and 382 rpm, and (c) 25 N and 891 rpm

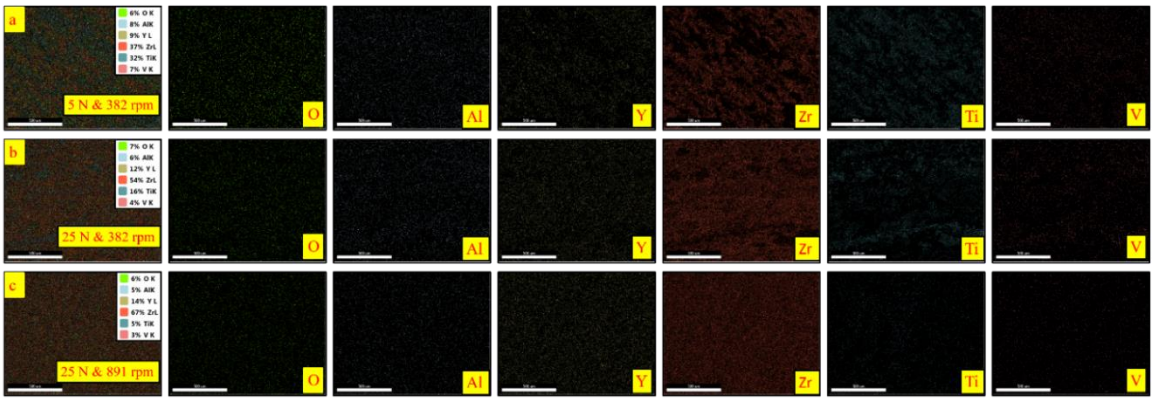

Figure 6.18 Elemental maps of worn surfaces of counter zirconia ball at: (a) 5 N and 382 rpm, (b) 25 N and 382 rpm, and (c) 25 N and 891 rpm

6.1.5 Raman analysis of wear surfaces of the conventional and L-PBF samples in different orientations

Figure 6.19 (a-d) shows the Raman spectra of wear track surfaces of the conventional, L-PBF AB-0°, L-PBF AB-45°, and L-PBF AB-90° after wear test at 5N and 382 rpm, at 5 N and 891 rpm, at 25 N and 382 rpm, at 25 N and 891 rpm, respectively. The spectra of worn samples show presence of TiO_2 in all the conventional and L-PBF samples at each load and sliding velocity. The formation of titanium oxide layers on surface of the samples, whose thickness is influenced by the sliding velocity and load during experiments.

Figure 6.20 (a-d) show the Raman spectra of wear track surfaces of the L-PBF HT-0°, L-PBF HT-45°, L-PBF HT-90°, and Raman peak values of all worn samples after wear test at 5N and 382 rpm, at 5 N and 891 rpm, at 25 N and 382 rpm, at 25 N and 891 rpm, respectively. For the conventional samples, more oxide layers are formed at 5 N load and 891 rpm sliding velocity in comparison with other load and sliding velocity conditions. Same trend is observed for the L-PBF as-built 0° oriented samples, but minimum oxide layer is formed at 25 N load and 382 rpm sliding velocity. In most of the samples, minimum oxide layers are formed at 25 N load and 382 rpm sliding velocity except in the conventional and L-PBF HT-90° samples.

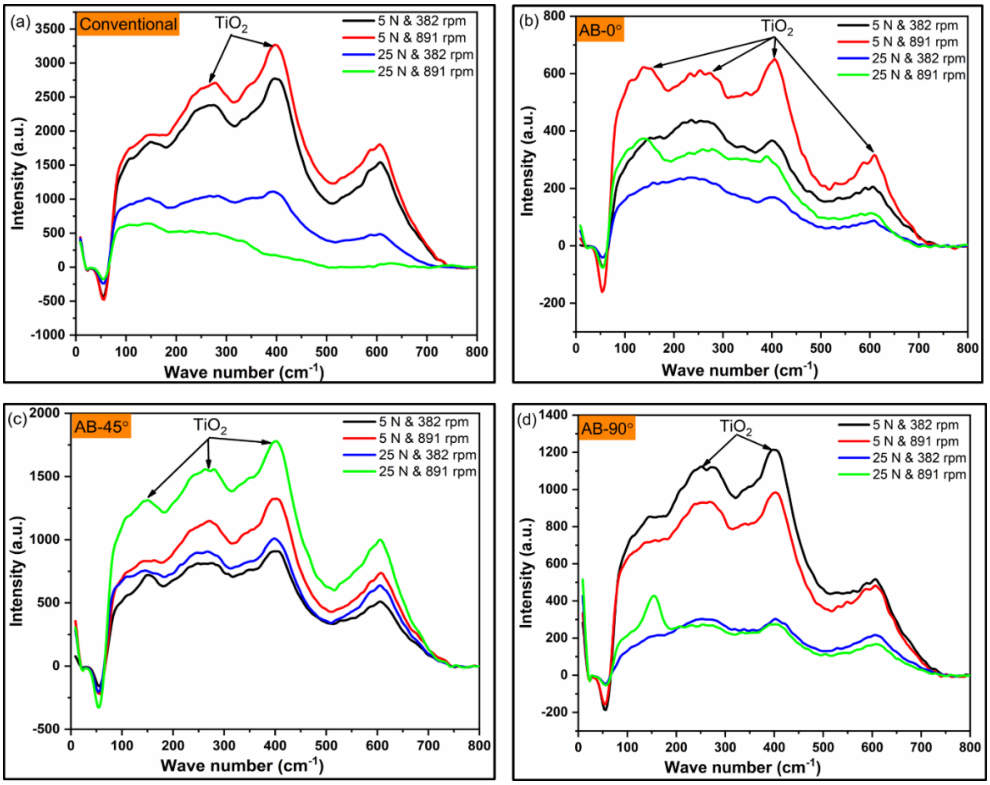

Figure 6.19 Raman spectra of wear track surfaces of: (a) conventional, (b) L-PBF AB-0°, (c) L-PBF AB-45°, and (d) L-PBF AB-90° samples

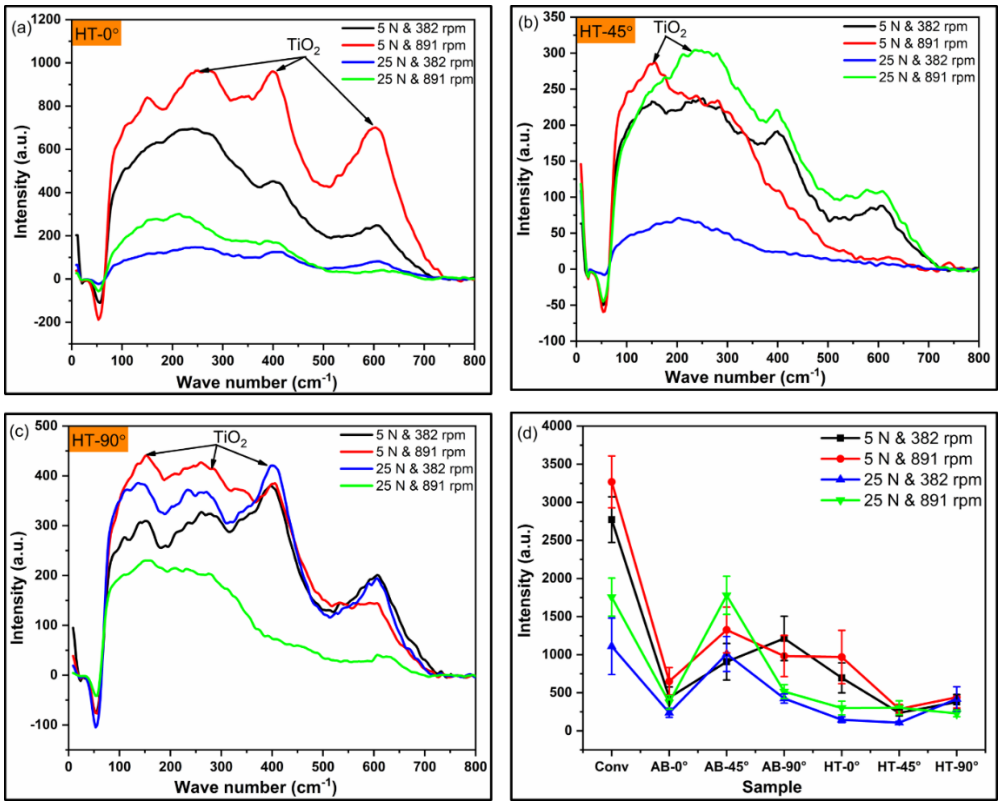

Figure 6.20 Raman spectra of wear track surfaces of: (a) L-PBF HT-0°, (b) L-PBF HT-45°, (c) L-PBF HT-90°, and (d) Raman peak values of all the wear samples tested in different conditions

Residual stress, microhardness variation, and microstructural anisotropy before wear test and the generation of titanium oxide during the wear test contribute significantly to the wear mechanisms observed in the both conventional and L-PBF Ti-6Al-4V samples. During L-PBF process, high cooling rate is experienced by each layer, and tensile residual stress is induced in the L-PBF fabricated samples. The maximum residual stress was observed in the 90° oriented L-PBF as-built samples, followed by 0° oriented and lowest in the 45° oriented samples. The tensile residual stresses were almost eliminated from the L-PBF samples after the heat treatment. The detailed explanation has been reported in the previously published paper [174]. The lower rate of wear in the HT condition with respect to that of the AB condition is due to the higher effective stress in the AB condition as compared to that in the HT condition, because of the presence of the tensile residual stresses in the AB condition.

For the constant load, with increase in sliding velocity, wear rate reduces but for the same sliding velocity, with increase in load, wear rate increases for the as-built and heat-treated conventional and L-PBF samples, in all the orientations. The wear track width and also the depth of the abrasion grooves are significantly less on the heat-treated L-PBF Ti-6Al-4V samples, tested at 5 N and 382 rpm sliding velocity, in comparison with the conventional and L-PBF as-built Ti-6Al-4V samples. At 25 N and 891 rpm, the wear track width and wear depth are maximum on the L-PBF HT-90° samples, which is comparable with that of the conventional samples.

Wear volume loss is high in the as-built samples compared to the heat-treated samples, at all load condition. This observation is in agreement with the higher microhardness values of the as-built samples. In this respect, the L-PBF as-built samples show a greater surface degradation, coherent with average wear rate (Figure 6.3). With increase in load,

the wear volume loss increases, which suggests a gradual transformation from mild wear to severe wear. Wear volume loss in the 90° oriented samples is more in comparison with that of the 0° oriented samples.

Therefore, the wear rate is maximum in the L-PBF 90° samples, followed by 0° and lowest in the 45° oriented samples, at 5 N load and 382 rpm sliding velocity (Figure 6.3 and Table 6.1). Same trend was observed also at 25 N load and 891 rpm sliding velocity. Likewise, a direct relationship was established between the residual stress and wear rate for the L-PBF as-built samples. The heat-treated samples exhibited the most favourable wear resistance owing to elimination of the residual stress after the treatment and formation of a protective oxide layer during the wear test.

Additionally, wear rate of the L-PBF as-built samples is higher than that of the conventional samples but after the heat treatment, wear rate of the L-PBF samples is comparable with that of the conventional samples (Table 6.1). As the build orientation increases, wear rate decreases first then increases in the as-built samples, but after the heat treatment, wear rate increases then decreases at low load and low sliding velocity.

In the L-PBF as-built samples, microhardness varied between 470 to 481 HV and the average value was 476 HV. After heat treatment, the microhardness is reduced but not in a significant manner. The average hardness of the L-PBF heat-treated samples was 449 HV. The detailed explanation has been reported in the previous paper [174]. The average hardness obtained for the specimens fabricated by the conventional process was 363 HV. For the L-PBF as-built specimens, the hardness value increased by 31.13 % and for the L-PBF HT samples, the hardness increased by 23.69 % and decreased by 5.67 % when compared to conventional and L-PBF AB samples respectively. According to Archard's linear law, hardness is inversely proportional to wear volume loss [154]. In our case, after

heat treatment, hardness is reduced and also wear volume loss is less, which contradicts the above law, as also found by Hua Li [155].

Oxidation is a common phenomenon observed in titanium alloys, and it has been observed to potentially reduce frictional forces between a plate and a zirconia ball. This reduction in friction can be attributed to a decrease in the coefficient of friction, essentially acting as a diffusion barrier between the titanium plate and the zirconia ball [151]. However, once the oxide film is disrupted, adhesive wear mechanisms come into play, causing attraction between the surfaces in contact, leading to relative motion.

Examination of worn surfaces in both the conventional and L-PBF Ti-6Al-4V samples, revealed plastic deformation due to adhesive wear and presence of grooves aligned with the direction of sliding, indicative of abrasive wear (Figure 6.6 - Figure 6.12). Additionally, more protection is exerted by the surface oxide formed on the Ti-6Al-4V heat-treated samples during wear test, which protects the subsurface layers against wear. At low sliding velocity, the wear track shows micro fragmentation process, at higher velocity, the brittle detachment of large particles occurs from the worn surfaces as clearly shown in Figure 6.6 - Figure 6.12. The wear rate is higher at 25 N load in each sample because of high heat generation and movable oxide particles (Figure 6.3, Figure 6.6 - Figure 6.12 (f)).

Based on the above facts, we can conclude that the formation of surface oxide is more dominant on the wear resistance than that of microhardness of the sample. Also, a clear relationship is established between the microstructural constituents, residual stress, hardness, and the wear behaviour of Ti-6Al-4V samples manufactured through conventional and L-PBF processes.

6.1.6 Biocompatibility of L-PBF Ti-6Al-4V samples fabricated in three different orientations

Cell culture is performed on 36 samples of the L-PBF Ti-6Al-4V samples fabricated in three different orientations of 0°, 45°, and 90°. Cell culture is performed effectively on 24 samples out of 36 samples, yielding positive cell culture results. The L-PBF Ti-6Al-4V samples showed enhanced corrosion resistance in Ringer's solution [213], as a result, their cell culture was further studied.

Figure 6.21 and Figure 6.22 present the fluorescence microscopic images of the MG-63 human bone osteosarcoma cells cultured on the L-PBF Ti-6Al-4V samples in the as-built and heat-treated conditions respectively. The cells are proliferated on all the L-PBF Ti-6Al-4V samples. On the as-built samples, more cells are adhered on the 45° oriented samples, followed by 0°, and minimum cells are adhered on the 90° oriented samples. After heat treatment, maximum cells are adhered on 45° oriented samples, followed by 90°, and minimum cells are adhered on the 0° oriented samples. The surface roughness of the 45° oriented component is highest among the three build oriented samples because of the higher accumulation of energy. Likewise, cell adhesion and growth are found to be highest in this orientation.

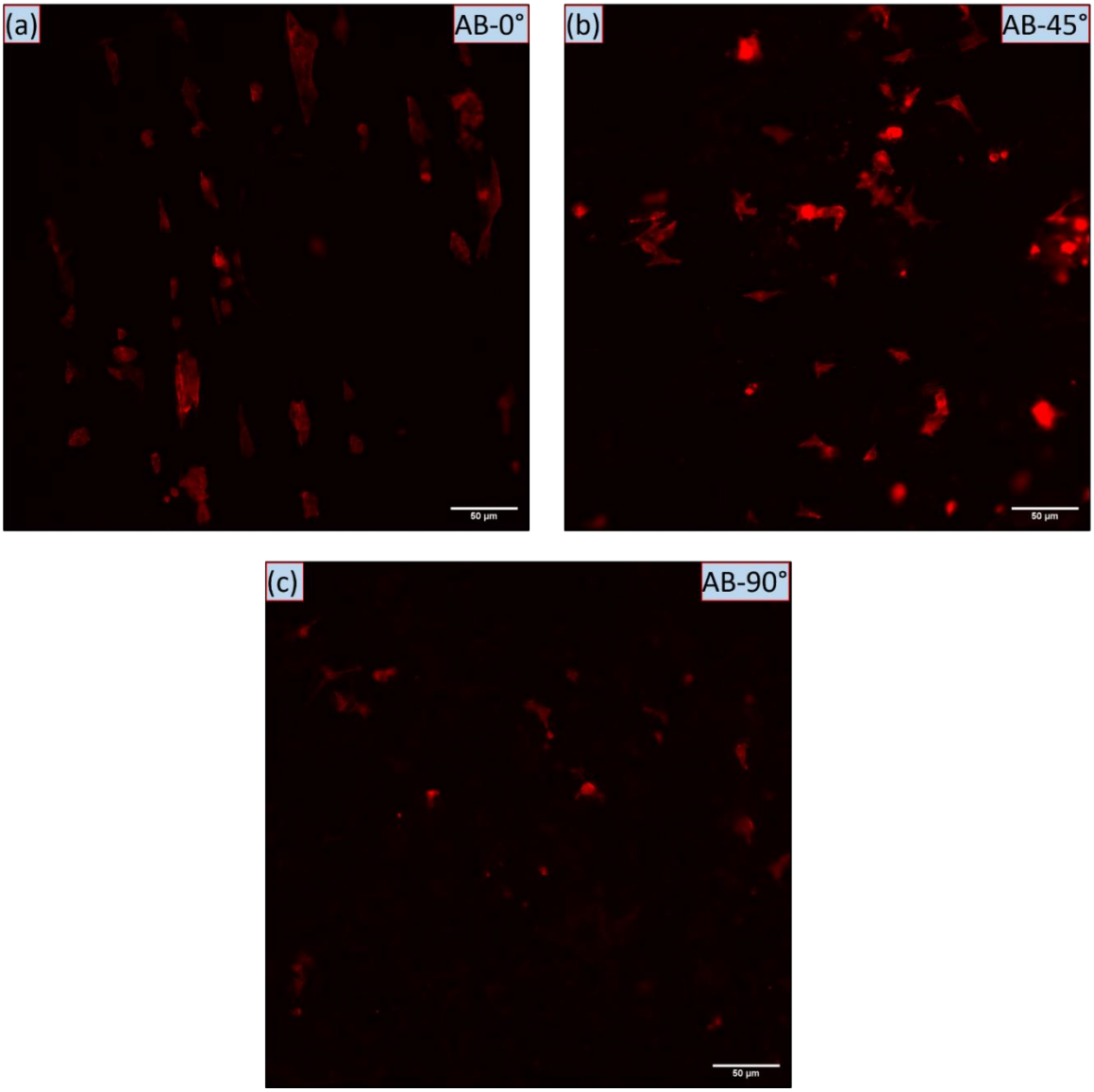

Figure 6.21 Fluorescent microscopic images of osteoblast (MG-63) rhodamine phalloidin over L-PBF Ti-6Al-4V as-built samples in different orientations: (a) 0°, (b) 45°, and (c) 90°

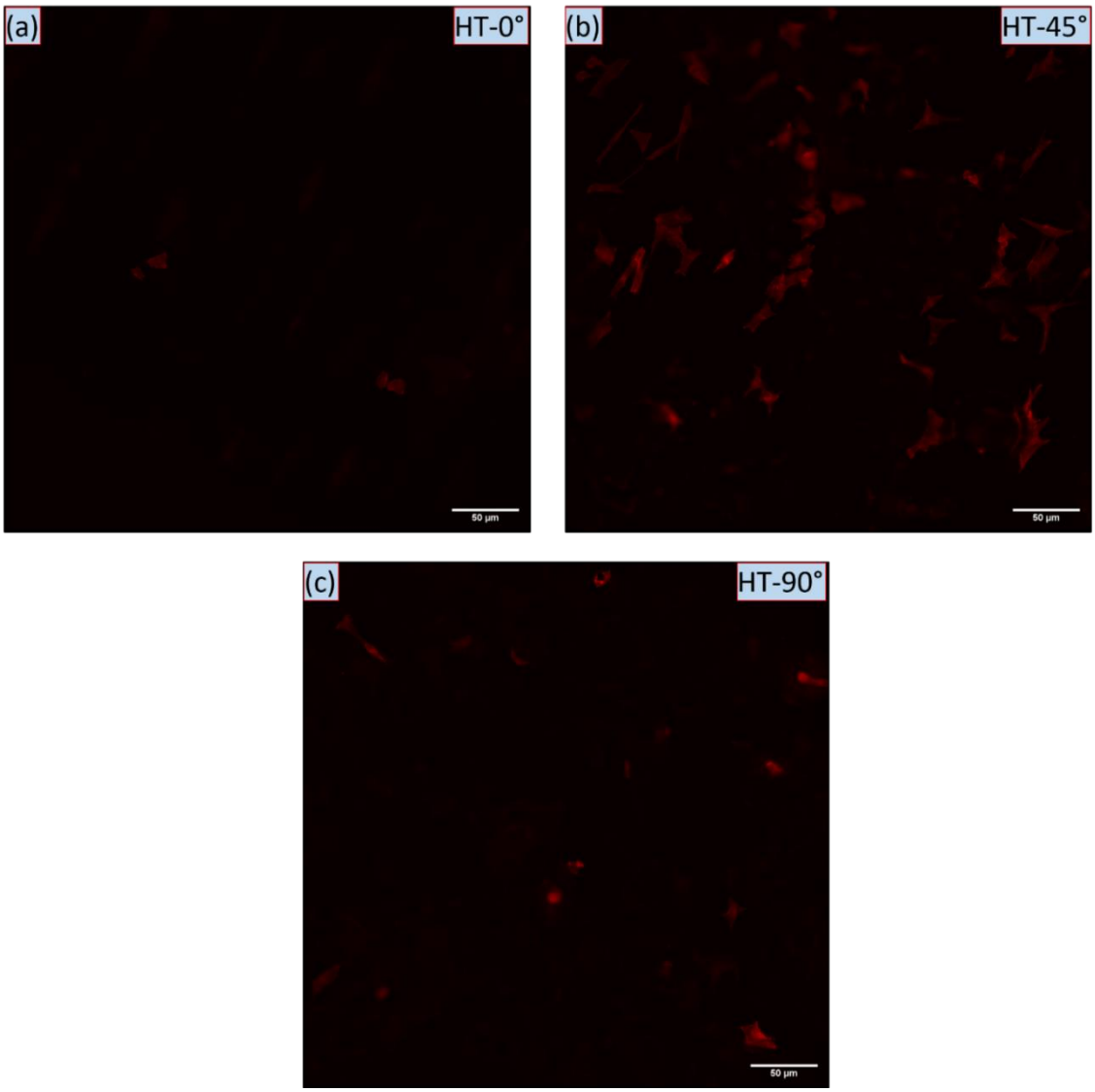

Figure 6.22 Fluorescent microscopic images of osteoblast (MG-63) rhodamine phalloidin over L-PBF Ti-6Al-4V heat-treated samples in different orientations: (a) 0°, (b) 45°, and (c) 90°

With the above results and discussion of wear and biological behaviour of AM fabricated Ti-6Al-4V alloy, conclusions and future scopes of mechanical, corrosion, and biological behaviour of AM fabricated Ti-6Al-4V alloy has been discussed in chapter 7.